

# Galaxy Morphological Classification with Manifold Learning

Vasyl Semenov<sup>a</sup>, Vitalii Tymchyshyn<sup>a,b</sup>, Volodymyr Bezguba<sup>a</sup>, Maksym Tsizh<sup>c,d</sup>

<sup>a</sup>*Kyiv Academic University, Vernadsky Blvd. 36, Kyiv, UA-03142, Ukraine*

<sup>b</sup>*Bogolyubov Institute for Theoretical Physics, Metrolohichna 14-b, Kyiv, UA-02000, Ukraine*

<sup>c</sup>*Astronomical Observatory of Ivan Franko National University of Lviv, Kyryla i Methodia str. 8, Lviv, 79005, Ukraine*

<sup>d</sup>*Dipartimento di Fisica e Astronomia, Università di Bologna, Via Gobetti 92/3, Bologna, 40121, Italy*

---

## Abstract

This paper describes applying manifold learning, the novel technique of dimensionality reduction, to the images of the Galaxy Zoo DECaLS database with the purpose of building an unsupervised learning model for galaxy morphological classification. The manifold learning method assumes that data points can be projected from a manifold in high-dimensional space to a lower-dimensional Euclidean one while maintaining proximity between the points. In our case, data points are photos of galaxies from the Galaxy Zoo DECaLS database, which consists of more than 300,000 human-labeled galaxies of different morphological types. The dimensionality of such data points is equal to the number of pixels in a photo, so dimensionality reduction becomes a handy idea to help one with the successive clusterization of the data. We perform it using Locally Linear Embedding, a manifold learning algorithm, designed to deal with complex high-dimensional manifolds where the data points are originally located. After the dimensionality reduction, we perform the classification procedure on the dataset. In particular, we train our model to distinguish between round and cigar-shaped elliptical galaxies, smooth and featured spiral galaxies, and galaxies with and without disks viewed edge-on. In each of these cases, the number of classes is pre-determined. The last step in our pipeline is k-means clustering by silhouette or elbow method in lower-dimensional space. In the final case of unsupervised classification of the whole dataset, we determine that the optimal number of morphological classes of galaxies coincides with the number of classes defined by human astronomers, further confirming the feasibility and efficiency of manifold learning for this task.

*Keywords:* galaxy morphology, unsupervised learning, topology

---

## 1. Introduction

The morphological galaxy classification stands among the oldest classification problems in astrophysics. Since the discovery of existing galaxies as separate structures of matter, people have noticed that they can be divided into several distinct morphological classes. The modern era of deep sky surveys with high-resolution imagery has brought variegation to this problem. Consequently, a significant number of attempts have emerged to apply different machine learning (ML) methods to help resolve it.

The Galaxy Zoo project has greatly facilitated exploring the possibilities of machine learning for the classification of galaxies. The Galaxy Zoo community did a fantastic job by creating a large, clean, and well-maintained human-labeled database of galaxy images from several surveys. The databases of the project have quickly become a test polygon of various ML models. From the simplest ones such as k-nearest neighbors (Shamir, 2009), support vector machines (Polsterer et al., 2012), and simple versions of neural networks (Banerji et al., 2010), to much more complicated ones, such as convolutional neural networks (Vavilova et al., 2022), and autoencoders (Xu et al., 2023).

In this work, we use one of the latest releases of the Galaxy Zoo project - Galaxy Zoo DECaLS (Walmsley et al., 2022). It was built on the Dark Energy Camera Legacy Survey data

and contains the classification of more than 300,000 galaxies. This particular database was also subjected to the numerous endeavors of machine-learning classification of galaxies. Consider some of the unsupervised models. The contrastive learning was used in (Wei et al., 2022). In (Fielding et al., 2022), the authors used a convolutional autoencoder feature extractor before applying k-means, fuzzy c-means, and agglomerative clustering to the extracted data features to cluster them. Lowering dimensionality was performed with this dataset in (Waghumbare et al., 2024) which was followed by the automated clustering algorithm. On the other hand, the manifold learning methods of dimensionality reduction, particularly the Locally Linear Embedding, haven't yet been used in any morphological classification in astrophysics. Instead, it was utilized when solving problems of galaxy (Vanderplas and Connolly, 2009), quasar (Jankov et al., 2020), stellar (Daniel et al., 2011), (Yude et al., 2013), and protostellar (Ward and Lumsden, 2016) spectra classification, as well as binary light curves classification (Bodi and Hajdu, 2021). Therefore, broadening the scope of its application appears to be an interesting enterprise.

This paper is structured in the following way. In section 2 we corroborate the concept of manifold learning. In section 3 we shortly describe the database, selection, and preprocessing procedures, then we explain in detail how we applied the method to the selected database, and present the results of classification.

We give a short conclusion in section 4.

## 2. Manifold learning

Manifold learning is a relatively novel method used to reduce the dimensionality of high-dimensional data keeping its underlying structure undisturbed. It assumes that data points lie on a lower-dimensional manifold embedded in the high-dimensional space. By learning the manifold, we can project the data onto this lower-dimensional space, reducing the number of features and making it easier to analyze.

There are several different methods like Multidimensional Scaling (MDS), Locally Linear Embedding (LLE), Isomap, etc. In this work, we employed the LLE algorithm.

In our case, the data points are images themselves. The original dimensionality is equal to the number of pixels in the image, and the brightness values define the position of a point on a high-dimensional manifold. As we will see below, the LLE method effectively decreases the dimensionality of such data by 2-3 orders while keeping similar images in proximity.

### 2.1. Locally Linear Embedding (LLE)

According to Roweis and Saul (2000), the Locally Linear Embedding (LLE) algorithm is constructed as follows. Given a set of  $N$  real-valued  $D$ -dimensional vectors  $\mathbf{x}_i$  sampled from a certain underlying manifold it is assumed that sampling density is sufficient to treat each data-point's neighborhood as a locally linear region of the manifold. The local structure of these regions can be captured through linear coefficients, which allow each data point to be represented as a linear combination of its neighbors.

If the data is distributed over a smooth, nonlinear manifold with an intrinsic dimensionality  $d < D$ , there is, to a close approximation, a linear transformation (involving translation, rotation, and scaling) that can map the high-dimensional coordinates of each neighborhood to a lower-dimensional manifold representation. The reconstruction weights  $W_{ij}$  by design capture intrinsic geometric characteristics of the data that remain invariant under such transformations. This invariance implies that the characterization of local geometry in the original high-dimensional space also holds in the manifold's local patches. Therefore, the same weights  $W_{ij}$  that reconstruct the  $i$ -th data point in  $D$  dimensions should also be effective in reconstructing its embedded representation in the lower-dimensional space.

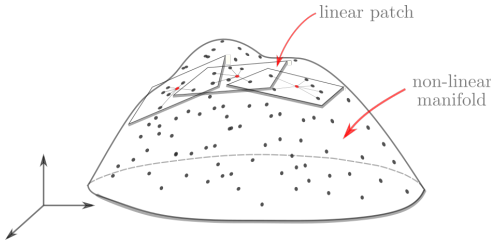


Figure 1: Locally Linear Embedding (LLE).

The high level outline of the algorithm is the following:

1. find  $k$  nearest neighbors for each data-point;
2. solve the minimization problem for reconstruction weights  $W$ ;
3. compute embedding coordinates  $Y$  using weights  $W$ .

Note that we try to minimize two loss functions one by one. On step 2 we want to minimize loss function

$$\epsilon(\{w_{ij}\}) = \sum_i \|\mathbf{x}_i - \sum_j w_{ij}\mathbf{x}_j\|^2 = \sum_i \left\| \sum_j w_{ij}(\mathbf{x}_i - \mathbf{x}_j) \right\|^2$$

with additional restriction  $\sum_j w_{ij} = 1$ . In essence we seek for

$$\{\hat{w}_{ij}\} = \operatorname{argmin}_{\sum_j w_{ij}=1} \epsilon(\{w_{ij}\})$$

On step 3 we want to minimize the loss function

$$\Phi(\{\mathbf{y}_i\}) = \sum_i \|\mathbf{y}_i - \sum_j w_{ij}\mathbf{y}_j\|^2,$$

we seek for

$$\{\hat{\mathbf{y}}_i\} = \operatorname{argmin}_{\{\mathbf{y}_i\}} \Phi(\{\mathbf{y}_i\}).$$

The latter basically allows for bijection  $\{\mathbf{x}_i\} \rightarrow \{\hat{\mathbf{y}}_i\}$  that is essentially a dimensionality reduction ( $\mathbf{x}_i \in \mathbb{R}^D$  and  $\hat{\mathbf{y}}_i \in \mathbb{R}^d$ ).

## 3. Experimental results

For the experimental investigation, we took 91481 colored images of galaxies in PNG format from the Galaxy Zoo Decals database Walmsley et al. (2022) for which the classification results by volunteer scientists were available. Each image constitutes a vector with  $424 \times 424 \times 3$  features. Examples of different types of galaxies are shown in Figure 2.

For better efficiency of galaxy classification, we extracted only the central part (120-by-120) from the images and converted it to grayscale.

Below we examined three examples of galaxy classification. For each example, there were selected only galaxies with 20 or more votes from scientists and at least one decision with less than 80% of all the votes. 50% of the images were used for training and 50% for independent testing. The LLE method was used to reduce the dimensionality of the images. Then the multinomial regression (MNR) was used for the classification and corresponding accuracy results for each dimensionality was shown.

### 3.1. Classification example 1

At first contemplate the classification of elliptical galaxies by "round"/"in-between"/"cigar" shapes (see Figure 3). A total of 8596 galaxies were used in this experiment (2690 "round", 4455 "in-between", 1451 "cigar").

Table 1 shows that the classification accuracy increases with the number of information components, reaching 95% when 100 information components (reduced "dimensions") are used. The corresponding confusion matrix is shown in Figure 4. Examples of classification performed by the algorithm are shown in Figure 5.

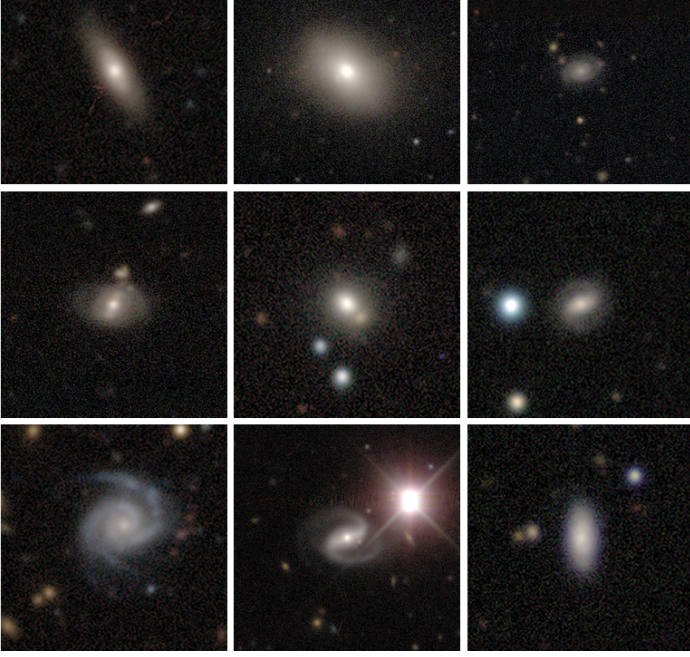


Figure 2: Example of images from Galaxy Zoo Decals database.

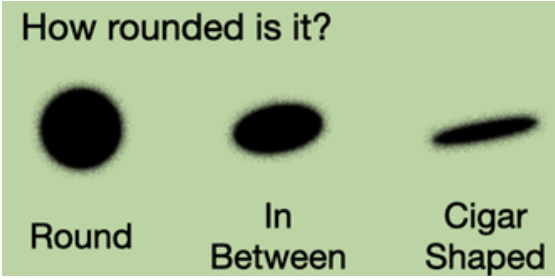


Figure 3: Schematic representation of “round”/“in between”/“cigar” galaxies (Walmsley et al. (2022)).

Dimensionality	Accuracy
1	0.52
2	0.59
3	0.61
5	0.86
10	0.91
20	0.93
50	0.93
100	0.95
200	0.94

Table 1: Dimensionality and corresponding MNR accuracy for LLE combined with MNR (first example).

For a more objective comparison, we also used two neural networks (without reducing the image dimensionality by manifold learning methods). First, we considered a feedforward neural network (NN) with two hidden layers with 128 and 64 ReLU-activated neurons respectively and an output layer with 3 softmax-activated neurons. The best accuracy obtained on the

True Class	Predicted Class		
	Cigar	In between	Round
Cigar	647	42	10
In between	52	2109	86
Round	4	93	1255

Figure 4: Confusion matrix for example 1.

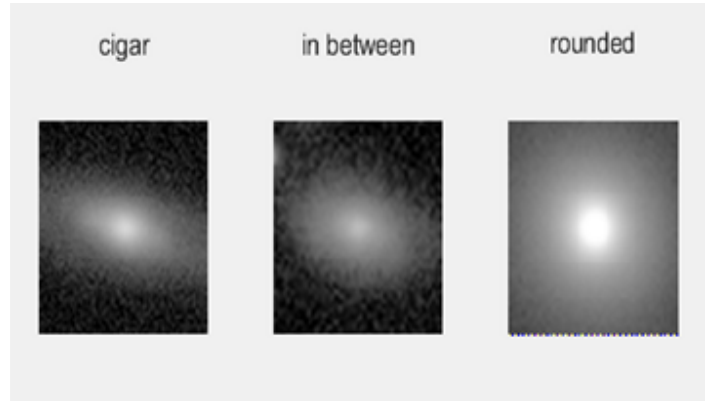


Figure 5: Example of galaxy classification by the proposed method.

test dataset (with batch size=32) was 85%, which is lower than the proposed method.

We also considered a multilayer Convolutional Neural Network (CNN) with 9 layers and 2861083 parameters which is specifically designed for image recognition. The best accuracy obtained by CNN on the test dataset (with batch size=32) was 95%, which is the same as our method based on data dimensionality reduction using the LLE method. This indicates the competitiveness of the proposed method with approaches designed specifically for image processing.

### 3.2. Classification example 2

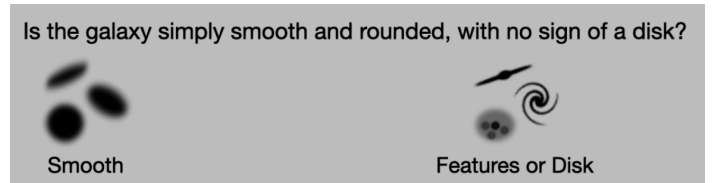


Figure 6: Explanation for “smooth”/“featured” galaxies (Walmsley et al. (2022)).

Next, contemplate the classification of spiral galaxies as “smoothed”/“featured” (see Figure 6). A total of 7213 galaxies were used in this experiment (3876 “smooth”, 3337 “featured”).

Dimensionality	Accuracy
1	0.53
2	0.57
3	0.59
5	0.58
10	0.62
20	0.72
50	0.78
100	0.8
200	0.82

Table 2: Dimensionality and corresponding MNR accuracy for LLE combined with MNR (second example).

Table 2 shows that the classification accuracy increases with the number of information components, reaching 82% when 200 information components are used. The corresponding confusion matrix is shown in Figure 7.

True Class	Featured	1277	393
	Smooth	270	1667
		Featured	Smooth
		Predicted Class	

Figure 7: Confusion matrix for example 2.

We also performed a comparison with two neural networks of the same architecture as before. The best accuracy obtained on the test dataset (with batch size=32) with feedforward NN was 76%, which is lower than the proposed method. CNN’s accuracy was 85%, which again is lower than our method (95%).

### 3.3. Classification example 3

And now consider the classification of galaxies as “edge on disk: yes”/“edge on disk: no” (see Figure 8). A total of 9628 galaxies were used in this experiment (1593 “disk edge: on”, 8035 “disk edge: off”).

Table 3 shows that the classification accuracy increases with the number of information components, reaching 95% when 200 information components are used. The corresponding confusion matrix is shown at the Figure 9.

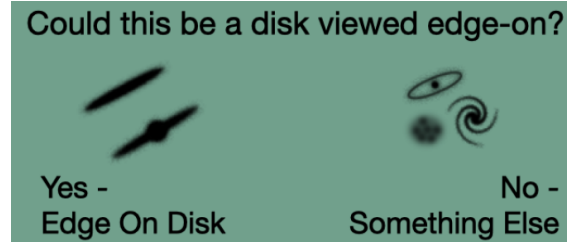


Figure 8: “edge on disk: yes”/“edge on disk: no” (Walmsley et al. (2022)).

Dimensionality	Accuracy
1	0.84
2	0.83
3	0.83
5	0.87
10	0.94
20	0.94
50	0.94
100	0.94
200	0.95

Table 3: Dimensionality and corresponding MNR accuracy for LLE combined with MNR (third example).

Feedforward NN network showed the accuracy of 93%, which again was lower than the method proposed by us, while CNN have 95% accuracy, – same as our method.

### 3.4. How many morphological classes are there actually?

Finally, we consider here the unsupervised classification of the general dataset without explicitly defining the number of classes using dimensionality reduction with LLE. In order to estimate the adequate number of information components that can be used to represent the image data using manifold learning, we applied the PCA method (which allows us to conveniently estimate information loss) to images of all types of galaxies. The result is shown in Figure 10. It shows that 99% of the information is retained with 32 components.

To estimate the number of galaxy classes present in the database, we applied the *silhouette* and *elbow* methods in combination with the k-means algorithm. The results are shown in Figure 11.

From Figure 11 we can conclude that the database contains about 5 types of galaxies, roughly corresponding to the existing classification of their types (elliptical, spiral, spiral with bar, lenticular, irregular). Details on Silhouette and Elbow methods of assessing the optimal number of clusters can be found in Appendix A. The code to reproduce all of our results can be found in public repository<sup>1</sup>

## 4. Conclusions and discussion

This paper presents the approach of applying the novel dimensionality reduction method, the Locally Linear Embedding,

<sup>1</sup><https://github.com/mtsizh/galaxy-morphology-manifold-learning>

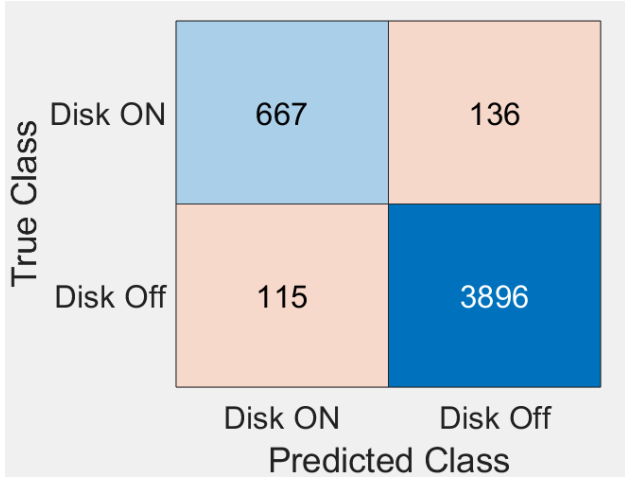


Figure 9: Confusion matrix for example 3.

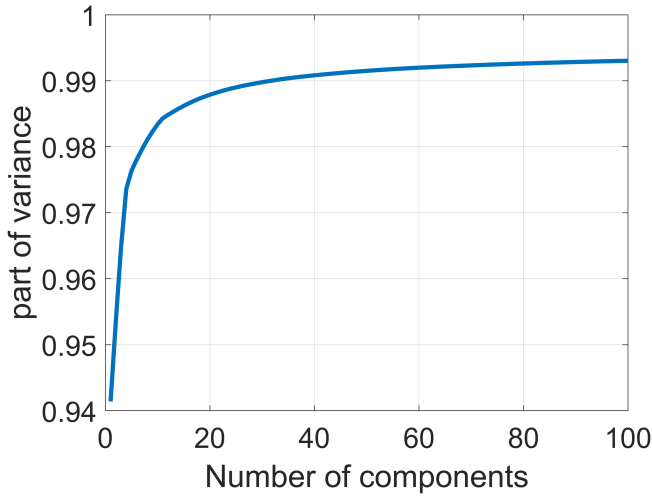


Figure 10: Dependence of the amount of preserved information on the number of information components.

to the large database of galaxy images, the Galaxy Zoo DECaLS. LLE is part of the wider family of methods, called manifold learning, which is meant to effectively simplify the complexity of data while keeping its important connections. With the reduced number of information components (dimensionality), we performed the morphological classification of galaxy images. Classification of reduced images morphological subclasses with multinomial regression shows competitive results even with almost no preprocessing of them. The accuracy reaches 95% for certain types of classification while being computationally much cheaper than more "traditional" techniques based on neural networks.

Our final step was unsupervised classification of the whole dataset with k-means using LLE-reduced images. With silhouette and elbow methods for finding the optimal k value in a k-means clustering algorithm, it gave a reasonable number of morphological galaxy classes, between 4 and 5, which coincides with the number of morphological classes that are recog-

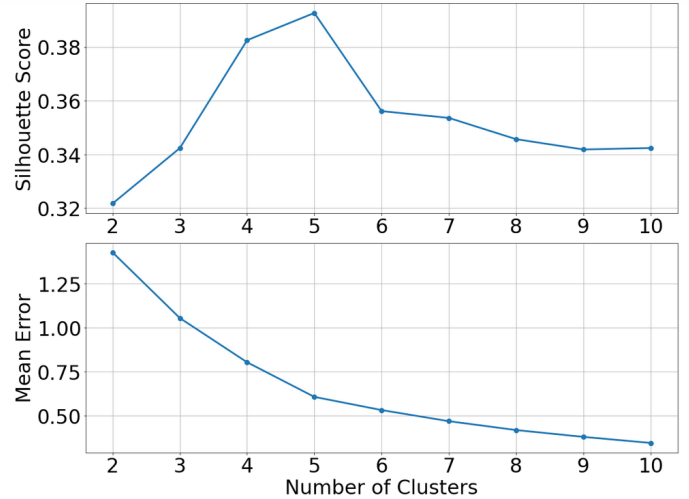


Figure 11: Dependence of the outputs of *silhouette* and *elbow* methods on the number of clusters.

nized by human astronomers (elliptical, spiral, spiral with bar or features, lenticular, irregular). This reaffirms a good fit of manifold learning methods for the task and shows nice potential for further development in this direction.

Hence, we can conclude, that LLE and manifold learning in general can become a handy tool for problems of galaxy or more generally, image morphological classification in astrophysics. There are some disadvantages of this method, in particular, it is not always obvious what dimensionality one should choose when reducing it, and often a hint from the outside method is needed. On the other hand, the advantages are more than clear: dealing with reduced data consumes much less computation power (all of presented here results can be obtained in few hours on average desktop computer), while the accuracy is competitive with other methods. The next steps in studying the application of LLE and manifold learning in this field could be more intense data filtration and preprocessing before feeding data to reduce dimensionality and the combination of manifold learning with more complex classification or clustering methods.

The nearest future of galaxy observation is quite promising. Already functioning telescopes such as Euclide (Euclid Collaboration et al., 2022) and James Webb Space Telescope (Treu et al., 2023) are expected to, or are already giving an astonishing new level of detalization when observing morphologies of galaxies. Moreover, a new kind of morphology classification will be needed with start of the observation of SKA (Braun et al., 2015). Therefore, developing diversified and miscellaneous classification pipelines for this problem is important. The one we propose here opens the way for mixing features from different wavelength. Among other merits are the possibility of making fast unsupervised classifications of morphology without having a heavy pre-trained model. Hence, we see a deep potential for developing this approach in the future.

## Acknowledgements

We would like to thank the Armed Forces of Ukraine for providing security to perform this work. This work was supported by the Ministry of Education and Science of Ukraine grant number 0122U001834 and by the National Academy of Sciences grant number 0120U101734.

## Appendix A. Description of Silhouette and Elbow methods for clustering

The silhouette method measures how similar a data point is to its own cluster compared to other clusters. It assesses both cluster cohesion (tightness of points within a cluster) and separation (distinctness between clusters).

For a data point  $i$ :

$$s(i) = \frac{b(i) - a(i)}{\max(a(i), b(i))},$$

where:

- $a(i)$ : Average distance from  $i$  to all other points in the same cluster.
- $b(i)$ : Average distance from  $i$  to all points in the nearest neighboring cluster.
- $s(i)$ : Silhouette score for point  $i$ , ranging from  $-1$  to  $1$ .

Interpretation:

- $s(i) \approx 1$ : Point  $i$  is well-clustered and far from other clusters.
- $s(i) \approx 0$ : Point  $i$  is on or near the boundary between two clusters.
- $s(i) \approx -1$ : Point  $i$  is poorly clustered and might belong to a different cluster.

The overall silhouette score for the clustering solution is the mean silhouette score across all data points:

$$\text{Average Silhouette Score} = \frac{1}{N} \sum_{i=1}^N s(i),$$

where  $N$  is the total number of data points.

The elbow method is used to determine the optimal number of clusters by analyzing the *within-cluster sum of squares* (WCSS), which measures the compactness of the clusters. For  $k$  clusters:

$$\text{WCSS} = \sum_{i=1}^k \sum_{x \in C_i} \|x - \mu_i\|^2,$$

where:

- $C_i$ : Cluster  $i$ .
- $\mu_i$ : Centroid of cluster  $C_i$ .

- $\|x - \mu_i\|^2$ : Squared Euclidean distance between a data point  $x$  and the cluster centroid  $\mu_i$ .

Elbow Point:

- As  $k$  increases, WCSS decreases because more clusters reduce compactness by assigning points closer to centroids.
- The "elbow point" is the  $k$  where the rate of decrease in WCSS sharply changes, indicating the optimal number of clusters.

## References

- Banerji, M., Lahav, O., Lintott, C.J., Abdalla, F.B., Schawinski, K., Bamford, S.P., Dan Andreescu, P.M., Raddick, M.J., Slosar, A., Szalay, A., Thomas, D., Vandenberg, J., 2010. Galaxy zoo: reproducing galaxy morphologies via machine learning. *Monthly Notices of the Royal Astronomical Society* 401, 342–353.
- Bodi, A., Hajdu, T., 2021. Classification of ogle eclipsing binary stars based on their morphology type with locally linear embedding. *The Astrophysical Journal Supplement Series* 225, id.1.
- Braun, R., Bourke, T., Green, J.A., Keane, E., Wagg, J., 2015. Advancing Astrophysics with the Square Kilometre Array, in: *Advancing Astrophysics with the Square Kilometre Array (AASKA14)*, p. 174. doi:10.22323/1.215.0174.
- Daniel, S.F., Connolly, A., Schneider, J., Vanderplas1, J., Xiong, L., 2011. Classification of stellar spectra with lle. *The Astronomical Journal* 142, 203.
- Euclid Collaboration, Bretonnière, H., Huertas-Company, M., Boucaud, A., Lanusse, F., Jullo, E., Merlin, E., Tuccillo, D., Castellano, M., Brinchmann, J., Conselice, C.J., Dole, H., Cabanac, R., Courtois, H.M., Castander, F.J., Duc, P.A., Fosalba, P., Guinet, D., Kruk, S., Kuchner, U., Serrano, S., Soubrie, E., Tramacere, A., Wang, L., Amara, A., Auricchio, N., Bender, R., Bodendorf, C., Bonino, D., Branchini, E., Brau-Nogue, S., Brescia, M., Capobianco, V., Carbone, C., Carretero, J., Cavuoti, S., Cimatti, A., Cledassou, R., Congedo, G., Conversi, L., Copin, Y., Corcione, L., Costille, A., Cropper, M., Da Silva, A., Degaudenzi, H., Douspis, M., Dubath, F., Duncan, C.A.J., Dupac, X., Dusini, S., Farrens, S., Ferriol, S., Fraiilis, M., Franceschi, E., Fumana, M., Garilli, B., Gillard, W., Gillis, B., Giocoli, C., Grazian, A., Grupp, F., Haugan, S.V.H., Holmes, W., Hormuth, F., Hudelot, P., Jahnke, K., Kermiche, S., Kiessling, A., Kilbinger, M., Kitching, T., Kohley, R., Kümmel, M., Kunz, M., Kurki-Suonio, H., Ligorì, S., Lilje, P.B., Lloro, I., Maiorano, E., Mansutti, O., Marggraf, O., Markovic, K., Marulli, F., Massey, R., Maurogordato, S., Melchior, M., Meneghetti, M., Meylan, G., Moresco, M., Morin, B., Moscardini, L., Munari, E., Nakajima, R., Niemi, S.M., Padilla, C., Paltani, S., Pasian, F., Pedersen, K., Pettorino, V., Pires, S., Poncet, M., Popa, L., Pozzetti, L., Raison, F., Rebolo, R., Rhodes, J., Roncarelli, M., Rossetti, E., Saglia, R., Schneider, P., Secroun, A., Seidel, G., Sirignano, C., Sirri, G., Stanco, L., Starck, J.L., Tallada-Crespí, P., Taylor, A.N., Tereno, I., Toledo-Moreo, R., Torradeflot, F., Valentijn, E.A., Valenziano, L., Wang, Y., Welikala, N., Weller, J., Zamorani, G., Zoubian, J., Baldi, M., Bardelli, S., Camera, S., Farinelli, R., Medinaceli, E., Mei, S., Polenta, G., Romelli, E., Tenti, M., Vassallo, T., Zacchei, A., Zucca, E., Baccigalupi, C., Balaguera-Antolínez, A., Biviano, A., Borgani, S., Bozzo, E., Burigana, C., Cappi, A., Carvalho, C.S., Casas, S., Castignani, G., Colodro-Conde, C., Coupon, J., de la Torre, S., Fabricius, M., Farina, M., Ferreira, P.G., Flose-Reimberg, P., Fotopoulou, S., Galeotta, S., Ganga, K., Garcia-Bellido, J., Gaztanaga, E., Gozaliasl, G., Hook, I.M., Joachimi, B., Kansal, V., Kashlinsky, A., Keihänen, E., Kirkpatrick, C.C., Lindholm, V., Mainetti, G., Maino, D., Maoli, R., Martinelli, M., Martinet, N., McCracken, H.J., Metcalf, R.B., Morgante, G., Morisset, N., Nightingale, J., Nucita, A., Patrizii, L., Potter, D., Renzi, A., Riccio, G., Sánchez, A.G., Sapone, D., Schirmer, M., Schultheis, M., Scottez, V., Sefusatti, E., Teyssier, R., Tutusaus, I., Valiviita, J., Viel, M., Whittaker, L., Knapen, J.H., 2022. Euclid preparation. XIII. Forecasts for galaxy morphology with the Euclid Survey using deep generative models. *Astronomy and Astrophysics* 657, A90. doi:10.1051/0004-6361/202141393, arXiv:2105.12149.

- Fielding, E., Nyirenda, C.N., Vaccari, M., 2022. The classification of optical galaxy morphology using unsupervised learning techniques. *International Conference on Electrical, Computer and Energy Technologies (ICECET) 20-22 July 2022, Prague-Czech*, 1–6.
- Jankov, I., Ilic, D., Kovacevic, A., 2020. Manifold learning in the context of quasar spectral diversity. *Proceedings of the XIX Serbian Astronomical Conference, October 13-17, 2020, Belgrade, Serbia* 100, 241–246.
- Polsterer, K.L., Gieseke, F., Kramer, O., 2012. Galaxy classification without feature extraction. *Astronomical Data Analysis Software and Systems XXI. Proceedings of a Conference held at Marriott Rive Gauche Conference Center, Paris, France, 6-10 November, 2011. ASP Conference Series* 461, 561.
- Roweis, S.T., Saul, L.K., 2000. Nonlinear dimensionality reduction by locally linear embedding. *science* 290, 2323–2326.
- Shamir, L., 2009. Automatic morphological classification of galaxy images. *Monthly Notices of the Royal Astronomical Society* 399, 1367–1372.
- Treu, T., Calabrò, A., Castellano, M., Leethochawalit, N., Merlin, E., Fontana, A., Yang, L., Morishita, T., Trenti, M., Dressler, A., Mason, C., Paris, D., Pentericci, L., Roberts-Borsani, G., Vulcani, B., Boyett, K., Bradac, M., Glazebrook, K., Jones, T., Marchesini, D., Mascia, S., Nanayakkara, T., Santini, P., Strait, V., Vanzella, E., Wang, X., 2023. Early Results From GLASS-JWST. XII. The Morphology of Galaxies at the Epoch of Reionization. *The Astrophysical Journal* 942, L28. doi:10.3847/2041-8213/ac9283, arXiv:2207.13527.
- Vanderplas, J.T., Connolly, A.J., 2009. Reducing the dimensionality of data: Locally linear embedding of sloan galaxy spectra classification of galaxy morphology. *The Astronomical Journal* 138, 1365–1379.
- Vavilova, I., Khramtsov, V., Dobrycheva, D., Vasylenko, M., Elyiv, A., Melnyk, O., 2022. Machine learning technique for morphological classification of galaxies from sdss. ii. the image-based morphological catalogs of galaxies at 0.02 $\leq$ z $\leq$ 0.1. *Space Science & Technology* 28, 27—55.
- Waghumbare, A., Singh, U., Kasera, S., 2024. Diat-dscnn-eca-net: separable convolutional neural network-based classification of galaxy morphology. *Astrophysics and Space Science* 369, 38.
- Walmsley, M., Lintott, C., Géron, T., Kruk, S., Krawczyk, C., Willett, K.W., Bamford, S., Kelvin, L.S., Fortson, L., Gal, Y., et al., 2022. Galaxy zoo decals: Detailed visual morphology measurements from volunteers and deep learning for 314 000 galaxies. *Monthly Notices of the Royal Astronomical Society* 509, 3966–3988.
- Ward, J.L., Lumsden, S.L., 2016. Locally linear embedding: dimension reduction of massive protostellar spectra. *Monthly Notices of the Royal Astronomical Society* 461, 2250–2256.
- Wei, S., Li, Y., Lu, W., Li, N., Liang, B., Dai, W., Zhang, Z., 2022. Unsupervised galaxy morphological visual representation with deep contrastive learning. *Publications of the Astronomical Society of the Pacific* 134, 114508.
- Xu, Q., Shen, S., de Souza, R.S., Chen, M., Ye, R., She, Y., Chen, Z., Ishida, E.E.O., Krone-Martins, A., Durgesh, R., 2023. From images to features: Unbiased morphology classification via variational auto-encoders and domain adaptation. *Monthly Notices of the Royal Astronomical Society* 526, 6391—6400.
- Yude, B., Jingchang, P., Bin, J., Peng, W., 2013. Stellar spectral subclass classification based on locally linear embedding. *Publications of the Astronomical Society of Japan* 65, 81.